Auxiliary Material for:

The use of radiocarbon to constrain current and future soil organic matter turnover and transport in a temperate forest

Maarten C. Braakhekke, Christian Beer, Marion Schrumpf, Altug Ekici, Bernhard Ahrens, Marcel R. Hoosbeek, Bart Kruijt, Pavel Kabat, and Markus Reichstein

[1]Max Planck Institute for Biogeochemistry, Jena Germany
[2]Earth System Science and Climate Change Chairgroup, Wageningen University, Wageningen, The Netherlands

Journal of Geophysical Research – Biogeosciences, 2013

Introduction

This PDF file contains auxiliary figures and tables for the study.

List of Figures

List of Tables

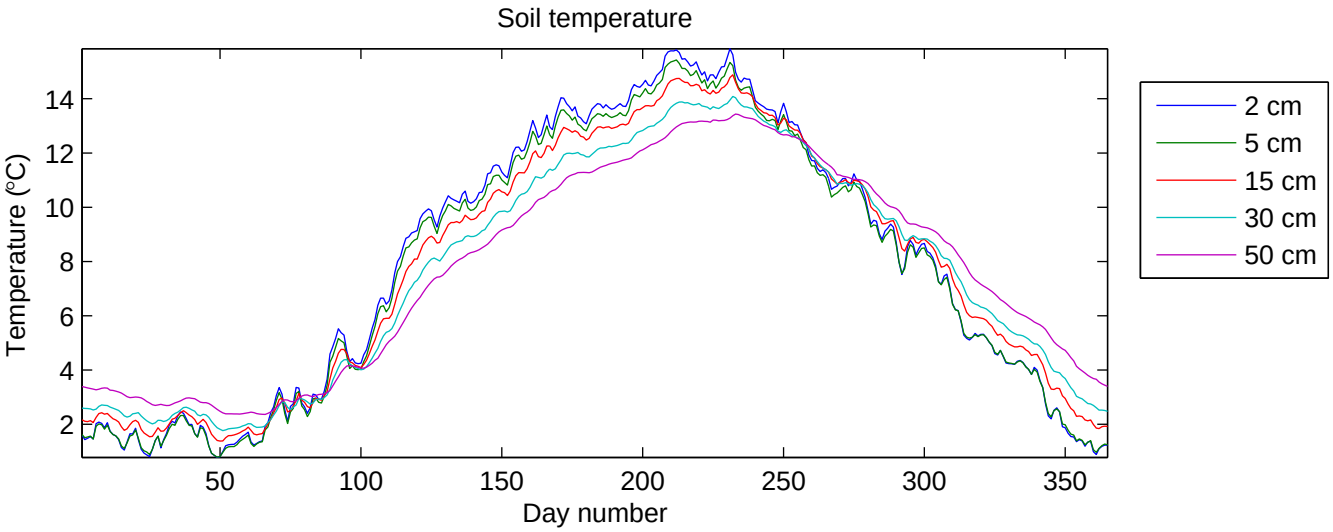

Figure 1: Average measured daily soil temperature at the study site Hainich as used in the simulation. Depths are relative to mineral soil surface. Temperatures are an average annual cycle based on half-hourly measurements in two profiles for the period 2000–2008. Note that for the simulation daily values are averaged to monthly.

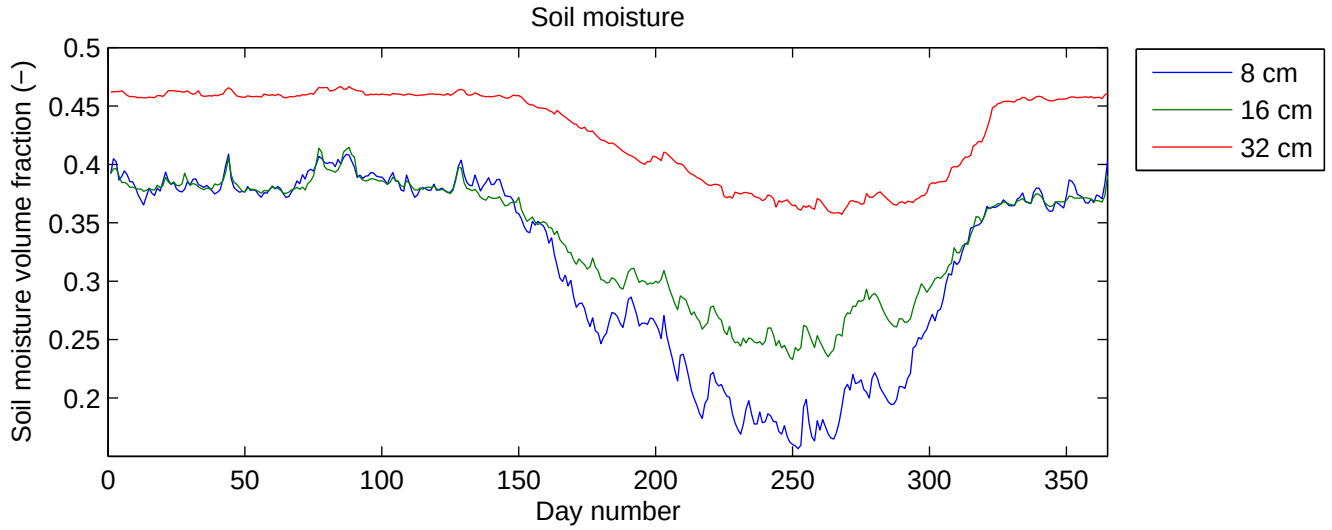

Figure 2: Average measured daily soil moisture at the study site Hainich as used in the simulation. Depths are relative to mineral soil surface. Moisture values are an average annual cycle based on half-hourly measurements for the period 2000–2008. Note that for the simulation daily values are averaged to monthly.

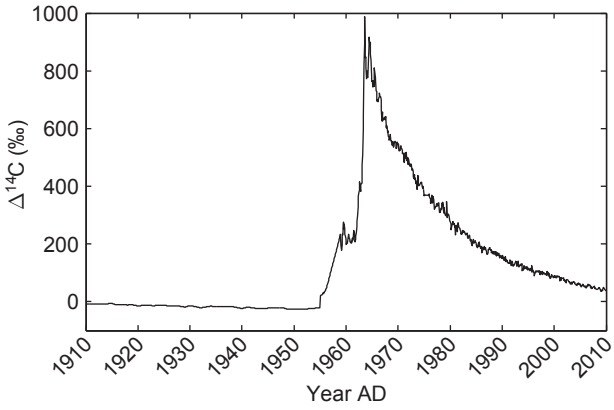

Figure 3: Atmospheric radiocarbon content used in the simulations.

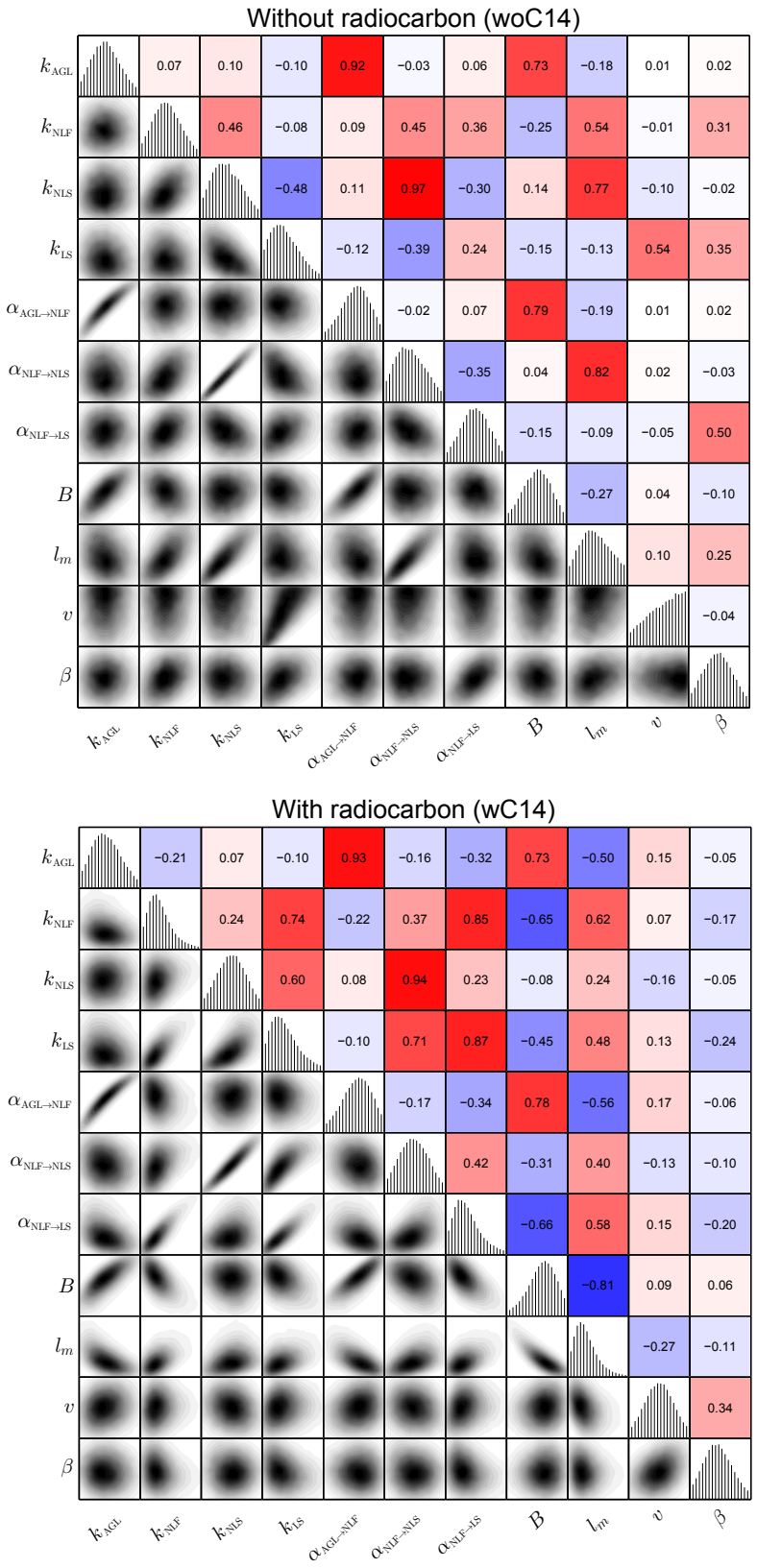

Figure 4: Correlation matrix of the posterior parameter distribution for the two calibrations. The figures show the correlations for each possible combination of two parameters. In the lower triangle bivariate probability density plots are depicted. In the upper triangle the correlation coefficients are shown, with blue indicating negative correlations and red positive correlations. On the diagonal histograms of the univariate marginal distribution for each parameter are shown.

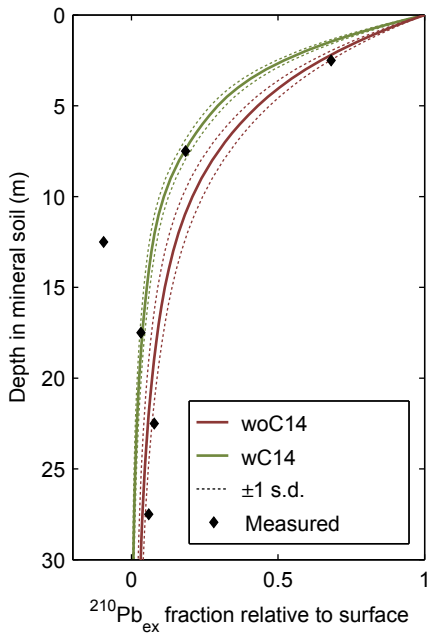

Figure 5: Measured lead-210 fractions relative to surface and corresponding model results. Model results are averages and standard deviations over the Monte Carlo ensembles.

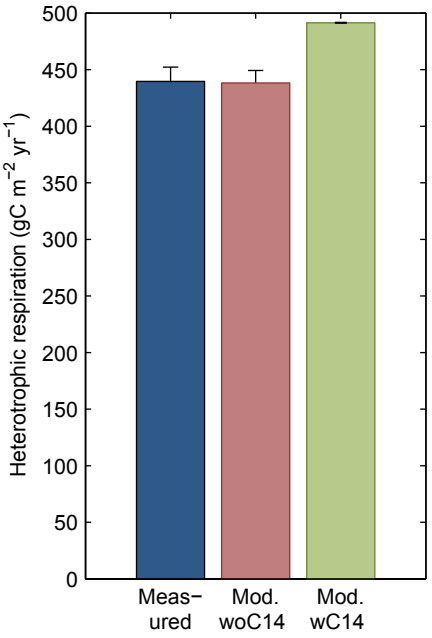

Figure 6: Measured and modeled total annual heterotrophic respiration. Model results are averages and standard deviations over the Monte Carlo ensembles. Errorbars for the measurements indicate one standard error of the mean.

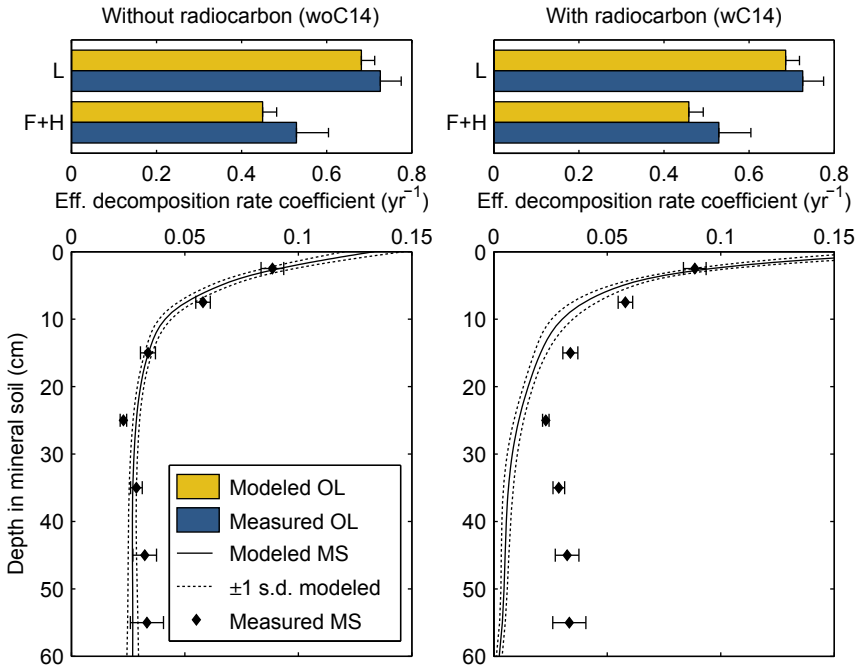

Figure 7: Measured effective decomposition rate coefficients and corresponding model results. Depicted model results are averages and standard deviations over the Monte Carlo ensemble. Errorbars for the measurements indicate one standard error of the mean.

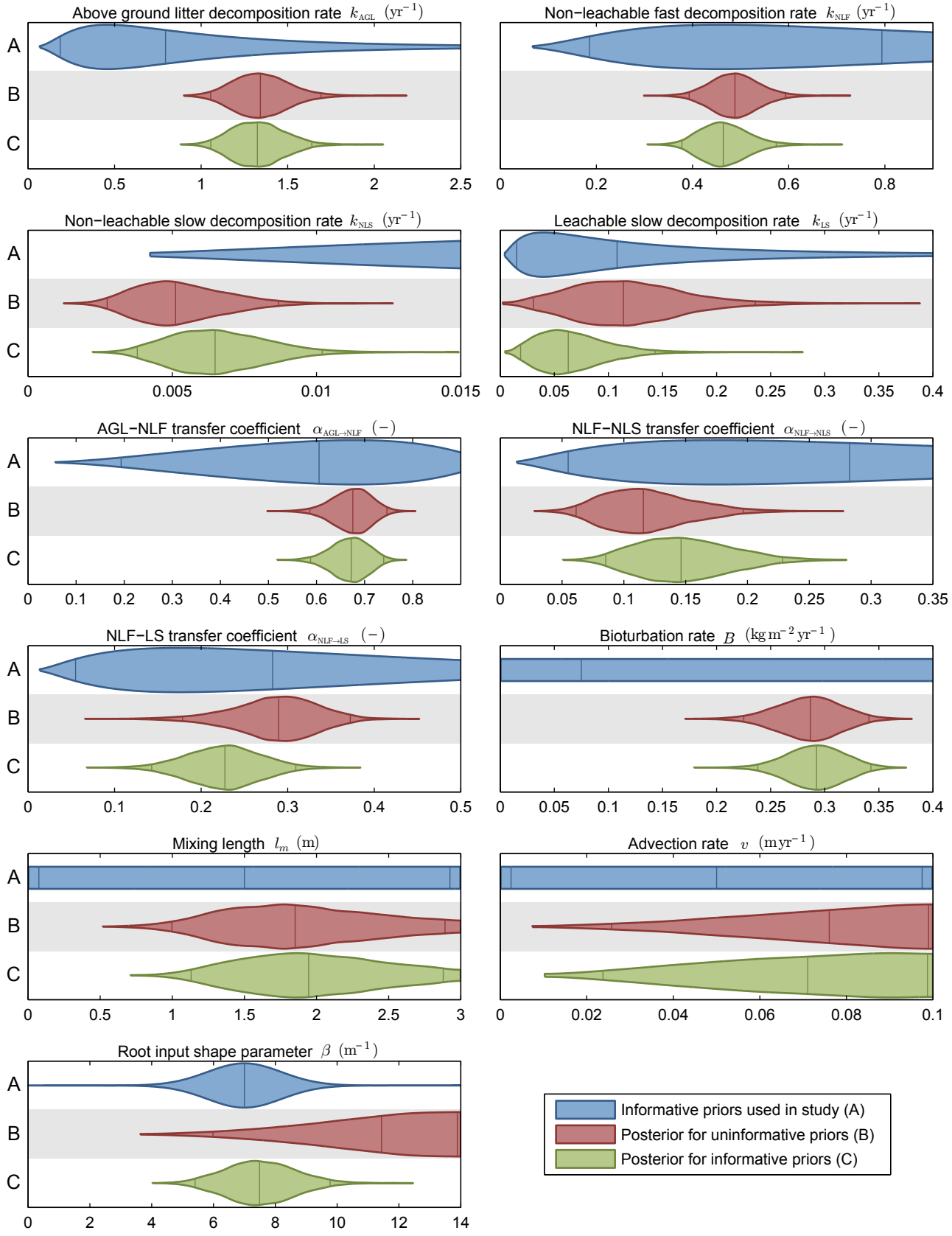

Figure 8: Marginal distributions for the informative priors as used in the study (A); posterior for a calibration with uniform (uninformative) priors (B), and with the informative priors (C). Posteriors are for setup woC14. The differences between the distributions illustrate the effects of the informative priors on the posterior

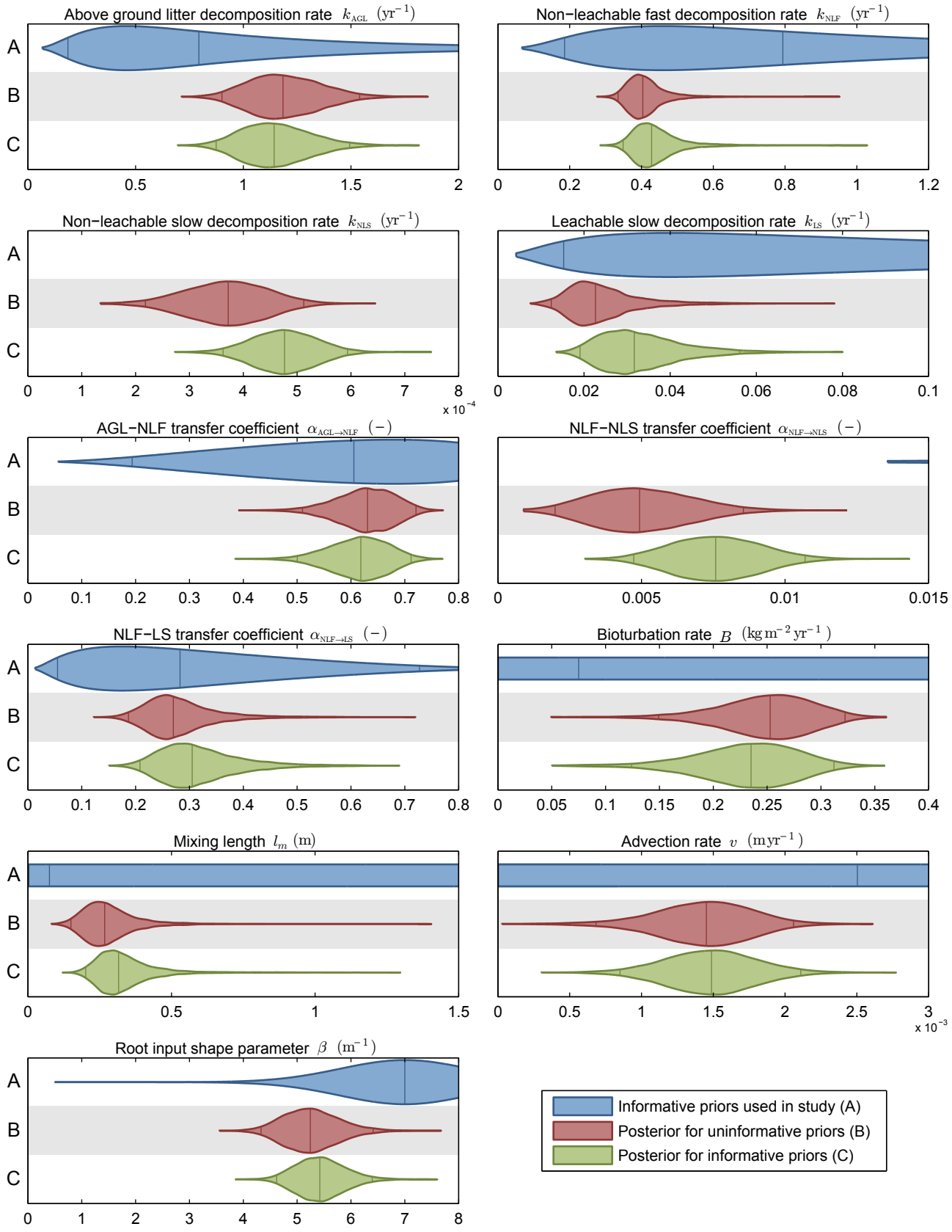

Figure 9: Marginal distributions for the informative priors as used in the study (A); posterior for a calibration with uniform (uninformative) priors (B), and with the informative priors (C). Posteriors are for setup wC14. The differences between the distributions illustrate the effects of the informative priors on the posterior

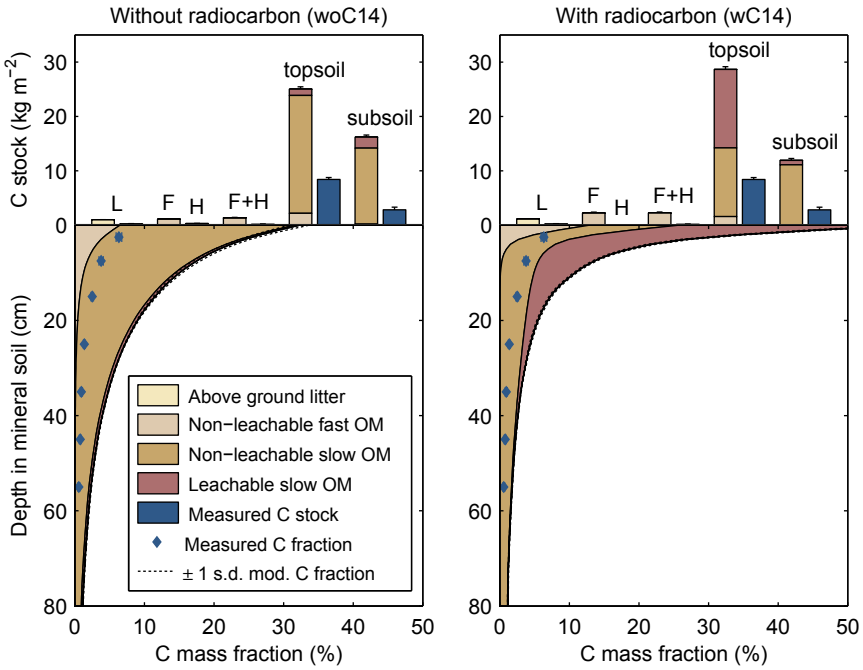

Figure 10: Organic carbon measurements for 2009 and corresponding model results based on JSBACH forcing. L, F, and H refer to the organic horizons; topsoil: 0–30 cm; subsoil: $>$ 30cm; OM: organic matter. All model results are ensemble means; errorbars denote one standard error of the mean for the measurements and one standard deviation (s.d.) for the model results.

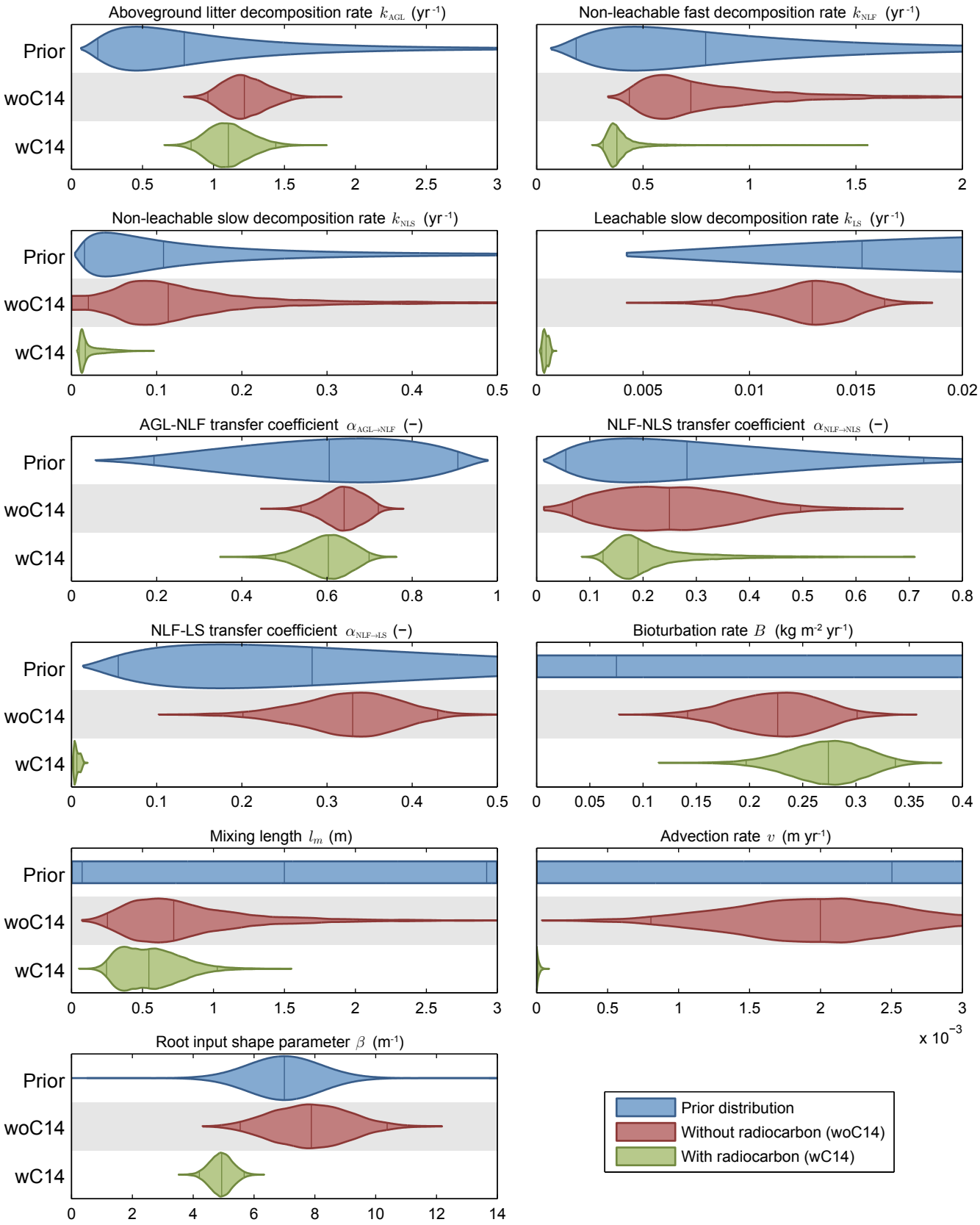

Figure 11: Violin plots marginal prior and posterior distributions for the sub-dominant mode. The three vertical lines inside the violins indicate the median and the 95% confidence bounds.

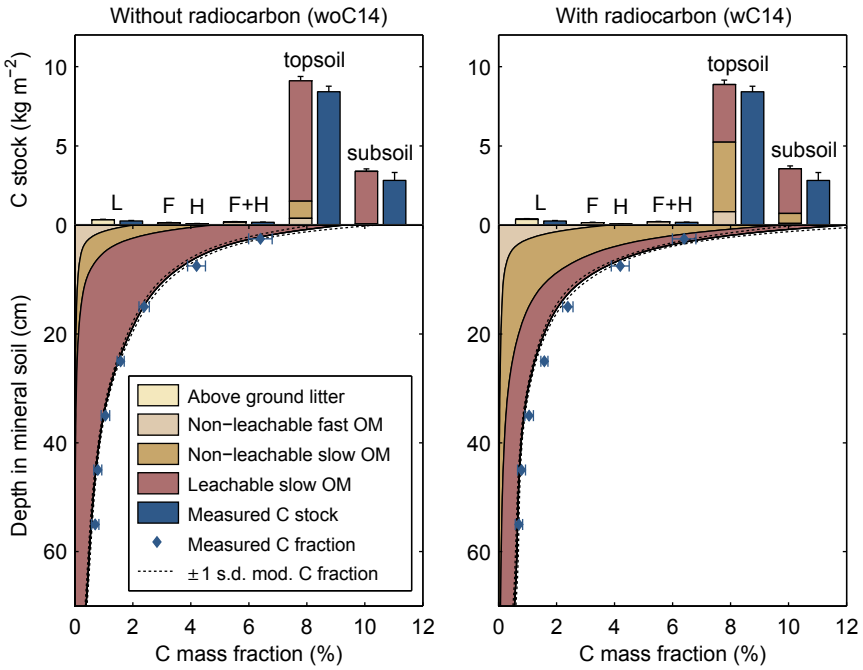

Figure 12: Organic carbon measurements and corresponding model results based on samples from the sub-dominant mode. L, F, and H refer to the organic horizons; topsoil: 0–30 cm; subsoil: > 30 cm; OM: organic matter. All model results are ensemble means; errorbars denote one standard error of the mean for the measurements and one standard deviation (s.d.) for the model results.

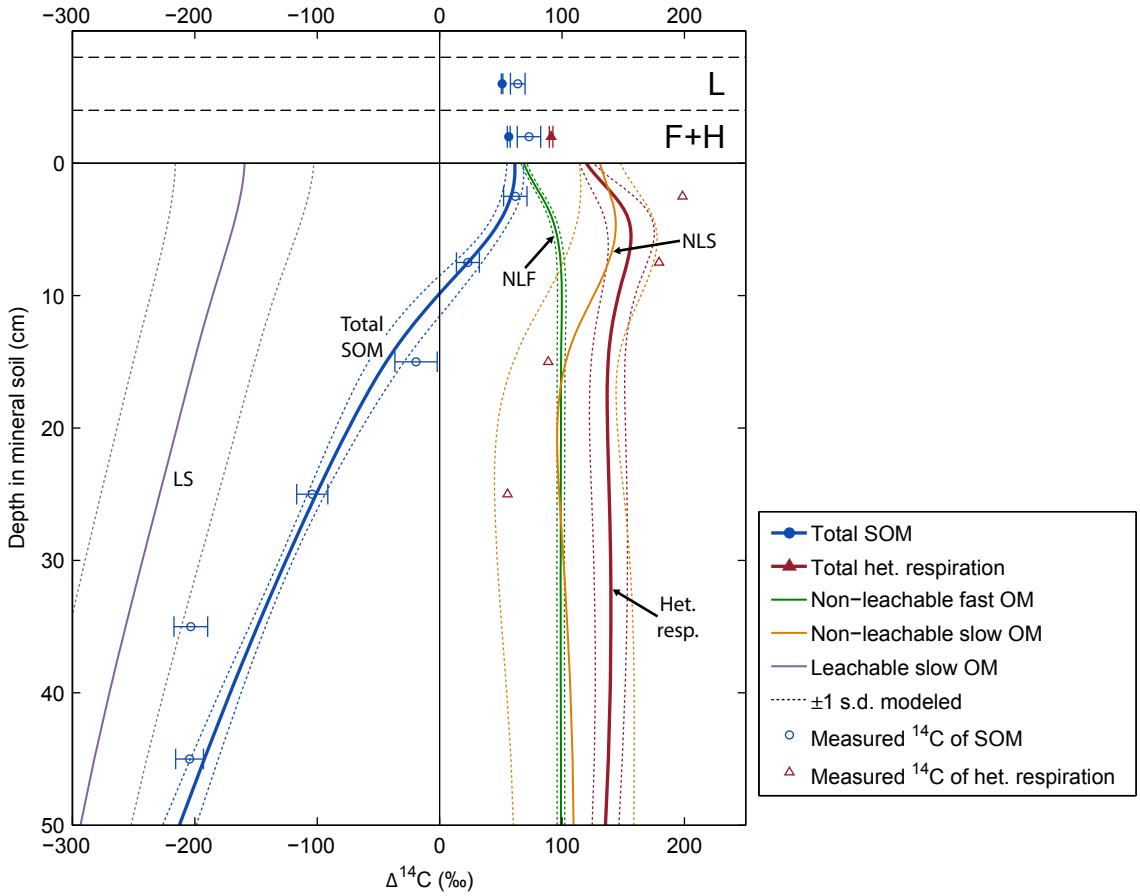

Figure 13: Measured Δ^{14}C for organic matter (March 2009) and heterotrophic respiration (April 2001) and corresponding model results based on samples from the sub-dominant mode for calibration wC14. Model results are means and standard deviation over the simulation ensemble. Additionally the Δ^{14}C values of the individual model pools (March 2009) are depicted. Note that the comparability between the OM Δ^{14}C and respiration Δ^{14}C is limited because they are shown for different years

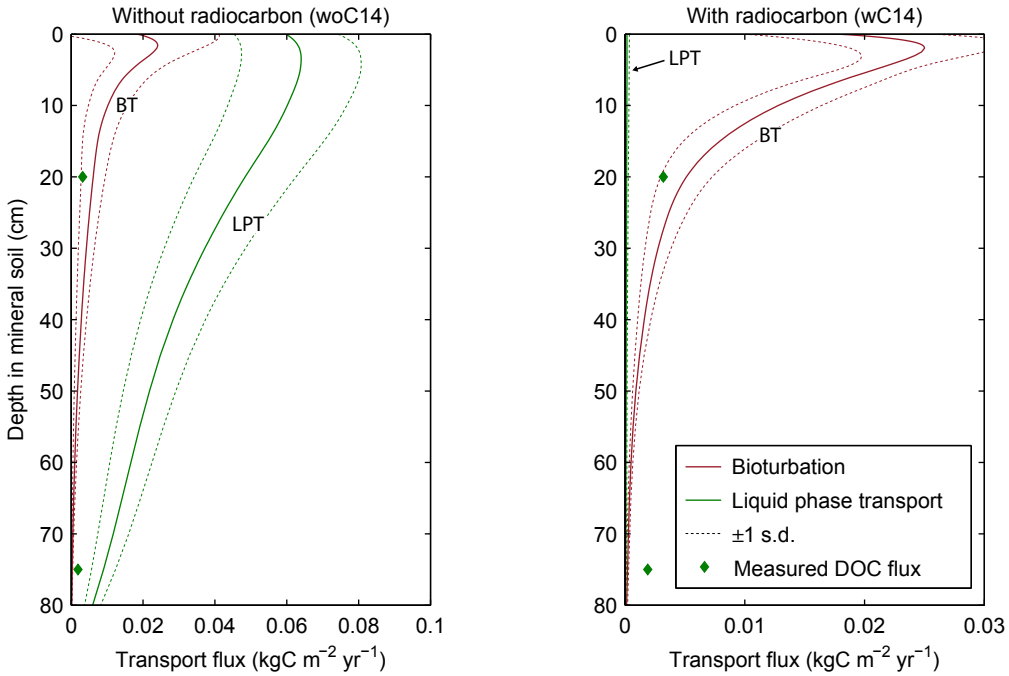

Figure 14: Modeled organic carbon transport fluxes based on samples from the sub-dominant mode and measured dissolved organic carbon fluxes. Model results are ensemble means and standard deviations averaged over the last simulation year. Measured DOC fluxes were taken from Kindler et al. (2011).

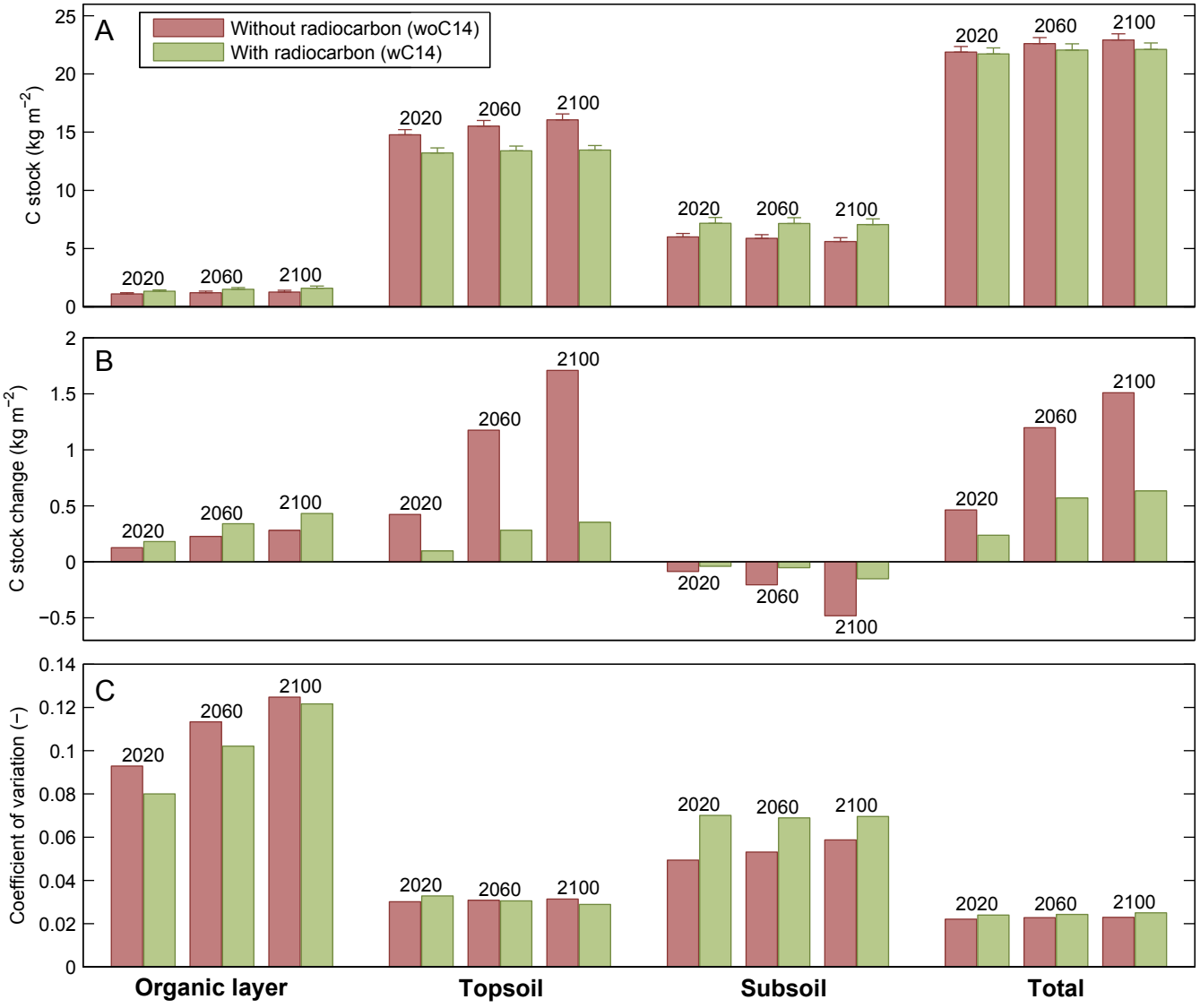

Figure 15: Modeled C stock results of projection until 2100 based on samples from the sub-dominant mode and JSBACH forcing data. A. total soil C stocks including standard deviation over the Monte Carlo ensemble. B. change in C stocks relative to values in 1980. C. coefficient of variation (standard deviation relative to mean) over the ensemble for the C stocks.

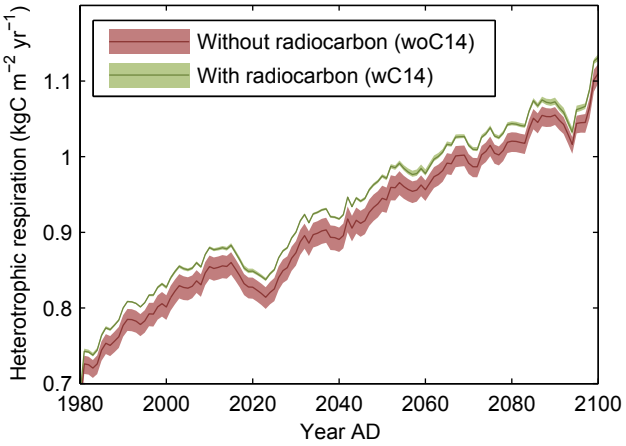

Figure 16: Modeled heterotrophic respiration for projection simulations until 2100 based on samples from the subdominant mode and JSBACH forcing data. Lines indicate ensemble means and shaded areas indicate 95% confidence bounds.

Table 1: Model driving data and not-estimated parameters.

Variable/Parameter	Value
Annual above ground litter input[a,b]	0.314 kg C m^{-2} yr^{-1}
Canopy	0.277 kg C m^{-2} yr^{-1}
Understory	0.037 kg C m^{-2} yr^{-1}
Total annual root litter input[a,b]	0.178 kg C m^{-2} yr^{-1}
Canopy	0.148 kg C m^{-2} yr^{-1}
Understory	0.03 kg C m^{-2} yr^{-1}
Average soil moisture[a,c,d]	0.361
Average soil temperature[a,c]	7.653 °C
Soil temperature response parameter	308.56[e] K
Soil moisture response parameter a[f]	1
Soil moisture response parameter b[f]	20
Bulk density L horizon	50 kg m^{-3}
Bulk density F horizon	100 kg m^{-3}
Bulk density H horizon[g]	150 kg m^{-3}
Bulk density mineral soil[a]	785.63–1350.3 kg m^{-3}
Bulk density pure mineral soil[h]	1300 kg m^{-3}
Initial depth of bottom boundary	0.7 m

[a] Only used in calibration simulations
[b] Kutsch et al. (2010); W. Kutsch (personal communication, 2009).
[c] Average over year and profile
[d] Fraction of maximum available water
[e] Lloyd and Taylor (1994)
[f] Soil moisture response function: $g(W) = \exp(-\exp(a - bW))$; (Subke et al., 2003).
[g] Also used in projection simulations as bulk density of pure organic soil
[h] Used in projection simulations to determine bulk density using pedotransfer function (Federer et al., 1993)

Mode	Setup		k_{AGL}	k_{NLF}	k_{NLS}	k_{LS}	$\alpha_{\mathrm{AGL}\to\mathrm{NLF}}$	$\alpha_{\mathrm{NLF}\to\mathrm{NLS}}$	$\alpha_{\mathrm{NLF}\to\mathrm{LS}}$	B	l_{m}	v	β
Dominant	woC14	2.5%	1.053	0.3779	0.003785	0.01896	0.5882	0.08471	0.1434	0.237	1.126	0.02322	5.394
		Opt.	1.366	0.4365	0.005664	0.06945	0.687	0.127	0.2254	0.3095	1.586	0.06497	7.231
		95%	1.645	0.5743	0.01019	0.1432	0.7397	0.2282	0.3107	0.3426	2.878	0.09868	9.791
	wC14	2.5%	0.8752	0.3487	0.0003618	0.01912	0.4991	0.004723	0.209	0.1229	0.202	0.0008569	4.603
		Opt.	1.187	0.3869	0.0004355	0.0239	0.6387	0.006184	0.2493	0.2758	0.2491	0.001373	5.269
		95%	1.492	0.6163	0.0005933	0.05653	0.7106	0.01071	0.5079	0.3116	0.6193	0.002104	6.404
Sub-dominant	woC14	2.5%	0.9565	0.4358	0.01979	0.008266	0.5378	0.06756	0.2009	0.1417	0.2563	0.0008034	5.54
		Opt.	1.282	0.5443	0.05198	0.01239	0.6548	0.1756	0.3003	0.2666	0.5779	0.002127	7.848
		97.5%	1.55	1.926	0.4966	0.01632	0.722	0.493	0.4304	0.3019	2.037	0.003415	10.35
	wC14	2.5%	0.8425	0.3129	0.009128	0.0002474	0.479	0.1248	0.002604	0.1968	0.2469	3.223e-07	4.206
		Opt.	1.074	0.3601	0.01264	0.000351	0.588	0.1741	0.004136	0.272	0.6864	4.939e-06	4.902
		95%	1.439	0.6858	0.06145	0.0007039	0.699	0.4644	0.01397	0.337	1.027	4.312e-05	5.679

Table 2: Properties of the marginal posterior distributions for both calibrations (with and without radiocarbon) and both modes. For each parameter the 2.5 % quantile, the sample with highest posterior density (Opt.), and the 97.5 % quantile are shown.

References

Federer, C. A., Turcotte, D. E., and Smith, C. T.: The organic fraction–bulk density relationship and the expression of nutrient content in forest soils, Canadian Journal of Forest Research-Revue Canadienne De Recherche Forestiere, 23, 1026–1032, 1993.

Kindler, R., Siemens, J., Kaiser, K., Walmsley, D. C., Bernhofer, C., Buchmann, N., Cellier, P., Eugster, W., Gleixner, G., Grunwald, T., Heim, A., Ibrom, A., Jones, S. K., Jones, M., Klumpp, K., Kutsch, W., Larsen, K. S., Lehuger, S., Loubet, B., McKenzie, R., Moors, E., Osborne, B., Pilegaard, K., Rebmann, C., Saunders, M., Schmidt, M. W. I., Schrumpf, M., Seyfferth, J., Skiba, U., Soussana, J. F., Sutton, M. A., Tefs, C., Vowinckel, B., Zeeman, M. J., and Kaupenjohann, M.: Dissolved carbon leaching from soil is a crucial component of the net ecosystem carbon balance, Global Change Biology, 17, 1167–1185, 2011.

Kutsch, W., Persson, T., Schrumpf, M., Moyano, F., Mund, M., Andersson, S., and Schulze, E.-D.: Heterotrophic soil respiration and soil carbon dynamics in the deciduous Hainich forest obtained by three approaches, Biogeochemistry, 100, 1–17, 2010.

Lloyd, J. and Taylor, J. A.: On the Temperature Dependence of Soil Respiration, Functional Ecology, 8, 315–323, 1994.

Subke, J. A., Reichstein, M., and Tenhunen, J. D.: Explaining temporal variation in soil CO_2 efflux in a mature spruce forest in Southern Germany, Soil Biology and Biochemistry, 35, 1467–1483, 2003.